

Laboratory Experiments on Suspended Sediment Concentration and Fluxes

Bosboom, Judith; Koomans, Ronald; Reniers, Ad

Publication date

1999

Document Version

Final published version

Published in

Proceedings of the 4th International Symposium on Coastal Engineering and Science of Coastal Sediment Processes

Citation (APA)

Bosboom, J., Koomans, R., & Reniers, A. (1999). Laboratory Experiments on Suspended Sediment Concentration and Fluxes. In N. C. Kraus, & W. G. McDougal (Eds.), *Proceedings of the 4th International Symposium on Coastal Engineering and Science of Coastal Sediment Processes* (1999 ed., Vol. 1, pp. 179-194). Article 13 American Society of Civil Engineers (ASCE).

Important note

To cite this publication, please use the final published version (if applicable).
Please check the document version above.

Copyright

Other than for strictly personal use, it is not permitted to download, forward or distribute the text or part of it, without the consent of the author(s) and/or copyright holder(s), unless the work is under an open content license such as Creative Commons.

Takedown policy

Please contact us and provide details if you believe this document breaches copyrights.
We will remove access to the work immediately and investigate your claim.

Green Open Access added to TU Delft Institutional Repository

'You share, we take care!' - Taverne project

<https://www.openaccess.nl/en/you-share-we-take-care>

Otherwise as indicated in the copyright section: the publisher is the copyright holder of this work and the author uses the Dutch legislation to make this work public.

LABORATORY EXPERIMENTS ON SUSPENDED SEDIMENT CONCENTRATION AND FLUXES

Judith Bosboom^{1,2}, Ronald Koomans³, Ad Reniers^{1,2}

Abstract: Flume experiments were performed with random waves normally incident on a dissipative beach consisting of sediment with varying density. This paper presents the data collected during the part of the measurement programme with a bed consisting of sand. During the latter series, detailed measurements of instantaneous fluid velocities and sediment concentrations were made resolving the spatial structure (in both horizontal and vertical direction) of the velocity and concentration fields. The analysis and interpretation is aimed at identifying the relative importance of mean flow, long and short waves to the net sediment fluxes and transport. It is found that the oscillatory suspended sediment transport dominated by the short wave transport cannot be neglected. Secondly, attention is paid to the sediment response and its effect on the sediment fluxes. The net oscillatory fluxes are seen to critically depend on the phase shifts between velocity and concentration at each frequency.

INTRODUCTION

Within the framework of the EU-sponsored MAST-III SAFE project a programme of detailed measurements of hydrodynamics, sediment concentrations, sediment transport and sediment composition has been carried out in WL|DELFT HYDRAULICS' Scheldt flume. The objective of the study was twofold: 1) the generation of high quality and high resolution data on hydrodynamics and sediment transport dynamics on a natural 2DV beach under erosive conditions with special attention to near-bottom resolution; and 2) the generation of data of selective transport phenomena of minerals with

-
- 1) WL | DELFT HYDRAULICS (mailing adress), p.o. box 177, 2600 MH Delft, The Netherlands, phone +(31)152858585, fax +(31)152858582, email Judith.Bosboom@wldelft.nl, Ad.Reniers@wldelft.nl
 - 2) Netherlands Centre for Coastal Research (NCK), Department of Civil Engineering and Geosciences, Delft University of Technology, Delft, The Netherlands
 - 3) Nuclear Geophysics Division, Kernfysisch Versneller Instituut, Rijksuniversiteit Groningen, 9747 AA Groningen, The Netherlands

varying density. Koomans et al. (1999) focus on the second objective of the experiments, whereas this paper deals with the first objective and therefore addresses the first part of the experiments (Series A). In Series A the focus was on the collection of instantaneous velocity and concentration data at several locations along the beach profile and for varying distances from the sandy bed. The set-up of the measurement programme was so as to enable the identification of the spatial correlation (in both horizontal and vertical direction) of concentration, the time-dependent near-bottom response of the concentration to water velocity and the contribution of the various velocity components to the sediment fluxes. The test conditions and beach geometry were chosen according to test 1 of Roelvink and Stive (1989).

DESCRIPTION OF EXPERIMENTS

Wave flume, beach geometry and sediment properties

The experiments were conducted in a wave flume at WL | DELFT HYDRAULICS in 1998. The main dimensions of the flume are a length of 55 m, a width of 1 m and a height of 1 m. The flume, with walls made up of glass windows, is equipped with a remote controlled rail-guided carriage allowing automatic profile surveying. The experiments were performed on an initially plane, 1 in 40, beach consisting of dune sand with grain diameters $D_{10} = 0.09 \text{ mm}$, $D_{50} = 0.13 \text{ mm}$ and $D_{90} = 0.19 \text{ mm}$.

Wave generation

Random waves were generated in a water depth of approximately 70 cm by a wave board equipped with an active wave absorption system (Klopman, 1995), such that at the same time waves were generated and reflected waves were absorbed. The latter prevented the re-reflection of free long waves traveling offshore towards the wave board. The wave generation was according to a second-order Stokes wave theory. This second-order wave board control includes corrections for the suppression of spurious free subharmonic and superharmonic components. The random wave fields generated were of the Jonswap type with a peak enhancement factor of approximately 3.3 representing a young sea state as expected under normal sea conditions. An improved method for wave generation (Klopman, 1998) was used which is closer to the theoretical second order spectrum with respect to the energy content for frequencies larger than the peak frequency. The incident wave conditions at deep water (water depth $h = 0.7 \text{ m}$) are $H_{m,0} = 0.17 \text{ m}$ and $T_p = 2 \text{ s}$. The wave-board control signal repeated itself every 1820.44 seconds.

Instrumentation

Surface elevations were measured by six resistance-type wave height meters (WHM), four of which were installed with varying space lags in the horizontal part of the flume and stayed in the same position during all tests in Series A (see Figure 1). Two mobile measurement carriages were deployed (see Figure 2), each equipped with -at different distances across the flume- a wave gauge, an Acoustic Doppler Velocity meter (ADV), an Optical Suspended Solids Concentration meter (OPCON) and two suction tubes (about 60 cm apart across the flume) of 3 mm internal diameter connected to a pump.

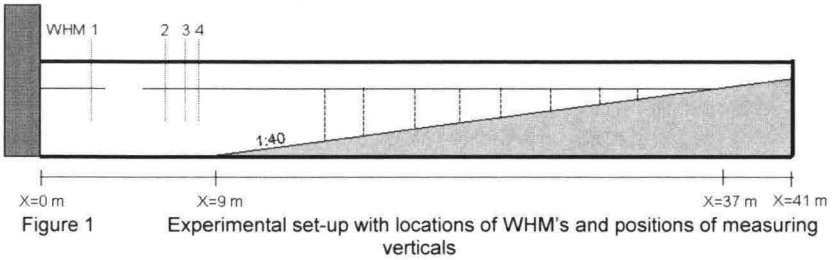


Figure 2 Measurement Carriage 1 during Series A equipped with -from left to right- suction tube (not visible), ADV, metal rod with PVC foot, OPCON, suction tube and WHM.

The vertical position of the ADV, OPCON and suction tubes could be varied relative to the measurement carriage, such that measurements could be performed at various positions above the bed. In addition, the carriages were equipped with a metal rod with on the lower end a PVC 'foot' which can be rotated in the x - z plane. In this way it can be placed on the sediment bed over the ripple structures, such that the distance of the instruments relative to the ripple height can be assessed using a measuring tape attached to the carriages. Carriage 1, equipped with an ADV with a sampling volume located 0.10 m below the probe tip, is located offshore of Carriage 2 which is equipped with an ADV with a sampling volume located 0.05 m below the probe tip enabling deployment at smaller water depths. The transverse suction tubes were connected to pumps that were sucking with a nozzle speed of 1.2 m/s. The extracted volume of

water and sediment respectively, is determined in a volume meter and converted to a time-mean concentration by weight using a calibration with a median grain size of $112\mu\text{m}$. The sediment collected with the suction system was analyzed on grain size using a settling tube.

Bottom profile variations were measured using the Profile Follower (PROVO). The instrument consists of a vertical gauge with a conductivity sensor at the bottom of the tip. The gauge moves vertically by means of a servo system so as to maintain a constant distance from the sediment bed. The statistical inaccuracy of the instrument is negligible compared to the inaccuracies associated with the natural variability of the bed in crosswise direction of the flume. To reduce this effect measurements were made as a standard procedure along two parallel trajectories, each running 33 cm from one side of the walls of the flume regularly supplemented with a trajectory in the center of the flume.

Measurement programme and acquisition of data

The total measurement duration of about 30 hours was divided in 'wave half-hours', subseries of approximately 35 minutes, during each of which an identical time series of random waves was generated. Measurements were taken during those 35 minutes by four fixed wave gauges which remained at the same position throughout the experimental programme and by instruments attached to a movable carriage. All movable instruments remained in a fixed horizontal and vertical position during the wave half-hour. The suction system was operated during the last 1820 s corresponding to the length of the steering signal. The post-processing of the time-dependent data also takes place for the last part of the time-series with the length of the steering signal. All instruments were sampled simultaneously at 50 Hz. In order to avoid aliasing, each signal was low-pass filtered by an analogue filter at 25 Hz before storage. A minimum of one bottom profile (using two or three trajectories) was sampled every 3.5 wave hours from which total load transport rates were inferred. The profile data were stored at 0.04 m intervals.

The first part of the Series A focused on the vertical structure of the concentration and velocity signal at eight characteristic locations along the profile ranging from $x = 15.5\text{ m}$ to $x = 30.5\text{ m}$ with a spacing of 2.5 m (see Figure 1). The vertical positions relative to the top of the ripples, z_{rel} , are chosen such that the sediment flux profile is approximately closed at the highest elevation from the bed. We have used $z_{rel} = 0.5, 1, 1.5, 2, 3, 4.5, 6\text{ cm}$ and in some cases 9 cm . From 25.5 m onwards, the water depth limitation of the ADV determines the highest elevation from the bed. Some measurements were repeated somewhat later in the test series in order to identify the variability of the data during the tests, especially that due to the changing bottom profile. In the second part, measurements were performed in order to assess the spatial coherence of the concentration on the scale of the wave orbital motion by deploying the two carriages at increasing horizontal distances. The latter procedure was performed for two characteristic locations along the profile (at $x = 20.5\text{ m}$ and $x = 25.5\text{ m}$, just offshore and onshore of the bar crest respectively) at one elevation above the bed ($z_{rel} = 1\text{ cm}$).

INTEGRAL SURFACE ELEVATION DATA

The surface elevation data shown in Figure 3 comprises set-up, significant wave height and cross-correlation coefficient between the low-pass filtered surface elevation and the wave envelope. The wave envelope is derived through high-pass filtering, squaring, de-meaning, and low-pass filtering of the elevation signal. Throughout this paper half the peak frequency (0.25 Hz) is used for the lowest short wave frequency. The lower plot of Figure 3 shows the initial bottom profile together with the single-barred bottom profile obtained after a total wave duration of approximately 30 hours.

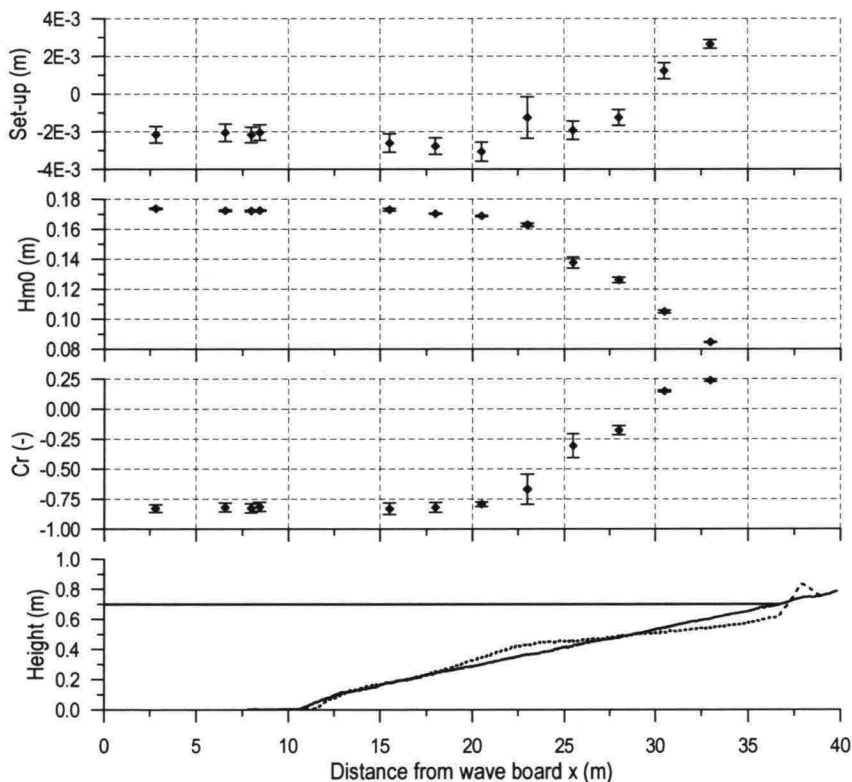


Figure 3 Set-up, significant wave height (H_{m0}), correlation coefficient (C_r) between wave envelope and long-wave surface elevation along profile and initial bed and bed after 30 hours (lower plot)

Figure 3 clearly shows the onset of breaking around $x = 18\text{ m}$ and the intensification of the breaking process around $x = 23\text{ m}$ from which point the wave height strongly reduces and a positive gradient is observed in the mean water level. From the bar crest onwards, the cross-correlation coefficient, which equals -1 in a complete bound long-wave situation, increases from the offshore value of -0.83 to 0.23 at the most landward measuring location. The changes in the correlation are explained by the increasingly

important short-wave modulation through the depth variations induced by the presence of the long waves for smaller depths.

During the 30 wave hours the surface elevation signal for the first four horizontal positions was recorded 48 times and, whereas for the 8 locations on the profile the recording of the surface elevation signal was repeated on average 10 times (ranging from 4 times at the most landward measuring location to 22 times at $x = 20.5\text{ m}$). The error bars in the upper three plots depict the standard deviation of the results for the respective location. The small standard deviation for the wave height at the various locations is satisfactory. Except for the stations around the bar crest, the variations in the cross-correlation coefficient between long wave surface elevation and wave envelope can for the greater part be explained from an increase of free long waves reflected from the beach as a result of the changing bottom profile. This can be seen from Figure 4 where the correlation coefficient for the fourth WHM is shown for all tests in chronological order. For the set-up, the variations can be largely attributed to the deployment of the suction system; during each measurement 8 buckets of water corresponding to 0.08 m^3 are withdrawn from the flume, whereas a variable amount of water is put back in the flume. The thus induced variations in the mean water level explain the variations in set-up for all points except for the location at the bar crest ($x = 23\text{ m}$). At the bar crest there is a large variation in the measured set-up which could not be seen to originate from the inaccuracies due to the suction system.

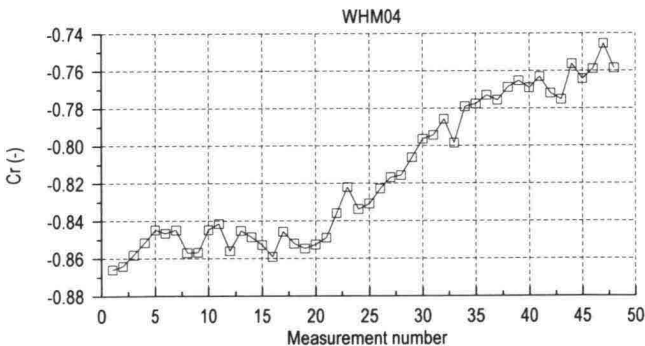


Figure 4 Development of cross-correlation coefficient between long wave surface elevation and wave envelope in time for WHM04

CROSS-SHORE FLOWS

Some characteristic time-averaged quantities derived from the near-bottom horizontal flow are given in Figure 5. For this figure, an arbitrary choice was made to use the signals recorded at 2 cm above the ripple crests. For $x = 20.5\text{ m}$ the measurement was performed twice, with an interval between the two measurements of 15 half hour measurements. The mean velocity (upper plot) is primarily due to the undertow, induced by wave breaking and can be seen to become larger in magnitude throughout the surf zone. A similar pattern is exhibited by the flow variance $\langle u_{lo}^2 \rangle$ in the low frequency range ($< 0.25\text{ Hz}$) as shown in the second plot. Note that the

brackets denote time-averaging over 1820 s.

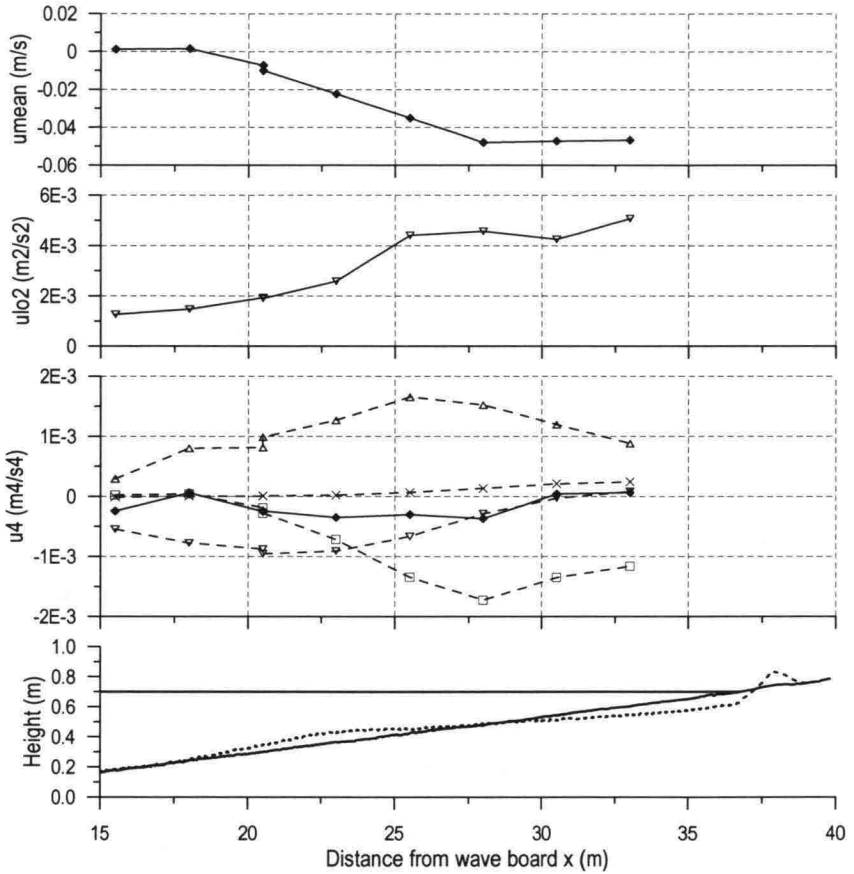


Figure 5 Flow characteristics along profile for $z_{rel} = 2 \text{ cm}$, mean flow (upper plot), long wave velocity variance (second plot), fourth velocity moment (third plot), total (diamond) and decomposed in short wave contribution (triangle up), interaction between long waves and short wave variance (triangle down), mean flow term (square) and rest term (cross), and initial bed and bed after 30 hours (lower plot)

In view of our interest in cross-shore sediment transport and realizing that many engineering net transport formulations contain terms proportional to some power of the near-bottom time-varying flow, i.e. $q \propto \langle u(t)|u(t)|^n \rangle$ with $n=3$ for suspended sediment transport according to the energetics approach (Bailard, 1981), the fourth velocity moment $\langle u(t)|u(t)|^3 \rangle$ is shown in the third plot. With the total velocity signal

consisting of a wave group averaged component $\langle u \rangle$, a short wave averaged oscillatory component u_{lo} and a short wave component u_{hi} and assuming that $\langle u \rangle \ll u_{lo} \ll u_{hi}$ and u_{hi} is uncorrelated to $\langle u_{lo}^2 \rangle$ and $\langle |u_{lo}|^3 \rangle$, we can approximate the fourth velocity moment as (see Roelvink and Stive, 1989):

$$\langle u(t)u(t)^3 \rangle \approx 4\langle u \rangle \langle |u_{hi}|^3 \rangle + 4\langle u_{lo} |u_{hi}|^3 \rangle + \langle u_{hi} |u_{hi}|^3 \rangle \quad (1)$$

The first term in Equation (1) is related to the return flow, the second term is nonzero only if there exists a correlation between the slowly varying velocity u_{lo} and the short-wave velocity variance u_{hi}^2 . The third term is nonzero in the case of a asymmetry about the horizontal plane caused by the nonlinearity of the waves.

Besides the total velocity moment the three contributions are given in the third plot. The crosses indicate the terms arising from the fact that u_{hi} is correlated to $\langle u_{lo}^2 \rangle$ and $\langle |u_{lo}|^3 \rangle$ close to the shoreline. As expected the term associated with the short wave asymmetry increases when the waves shoal and the short wave asymmetry is strongly reduced beyond the point of initial breaking. The interaction term between long wave velocity and short wave variance is negative along the first part of the profile where the group-bound waves are dominating and becomes positive as soon as the short-wave fluctuations due to a slowly varying water level become important. In the term associated with the mean flow, the pattern of the undertow and the short wave velocity variance is recognized.

SUSPENDED SEDIMENT CONCENTRATION

Calibration

The calibration of the suction system is determined by the trapping efficiency α , defined as the ratio of the sediment concentration in the sample over the concentration in the flow. Following Bosman et al. (1987), we assume the trapping efficiency to be constant and estimate α to lie in the range from 0.75 to 0.8. The extracted volume of water and sediment is determined and converted to a time-mean concentration by weight using a calibration with a median grain size of 112 μm .

Since the OPCON calibration is dependent on grain-size, for each measurement the OPCON calibration performed for the bed material is corrected for the effect of grain-size using the grain-size of the material as collected with the suction system in the respective measurement. Based on a series of OPCON calibrations performed with varying grain-sizes in a representative range, the multiplication factor for the concentrations determined using the calibration for the bed material is roughly estimated as $D_{50}/D_{50,bed}$ with $D_{50,bed} = 129 \mu\text{m}$. Figure 6 compares the so determined mean concentrations from the OPCON with the corresponding values determined from the suction system with $\alpha = 0.77$. The dotted line is the linear fit through the data points ($R^2 = 0.9$). The agreement is fairly well, especially considering the uncertainties

in for example the OPCON calibration and the dependency of the calibration on the grain-size as well as the uncertainties in the trapping efficiency and the error caused by the volume measurements of the sampled sediment.

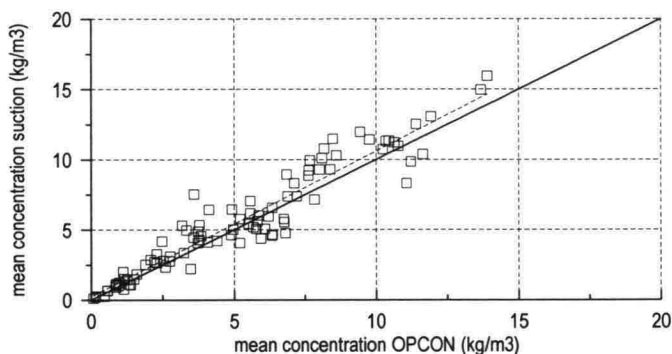


Figure 6 Comparison between mean concentration measured with the OPCON and determined from the suction system with $\alpha = 0.77$ for all measurements in series A

Time-mean load

In order to obtain the time-mean load along the profile, the time-mean concentration profiles are integrated over depth (see Figure 7, upper plot). On visual inspection of the mean concentration profiles, it appeared that all but the profiles for the two most shoreward stations are closed well. The load might therefore be somewhat underestimated for these two stations. It can be seen that the load increases as the wave shoals, reaching a maximum around the top of the bar where the highest waves are breaking, from where on, despite the increased turbulence in the surf zone, the load decreases with decreasing wave height.

NET TRANSPORT RATES

Transport obtained from profile deformation

Net transport rates have been inferred from profile deformation by applying the continuity equation for the sediment volume assuming the porosity of the bed material to be constant:

$$(1-n) \frac{\partial z_b}{\partial t} + \frac{\partial \langle q \rangle}{\partial x} = 0, \quad (2)$$

where n is the porosity of the bed material, z_b is the bed level and $\langle q \rangle$ is the time-averaged rate of volume transport in x -direction. The differential equation is solved assuming closure at the horizontal part of the flume. The thus derived transport rates are shown in Figure 7 (second plot, drawn line) for which the measured bottom profiles after about 8 and 26 hours respectively were used.

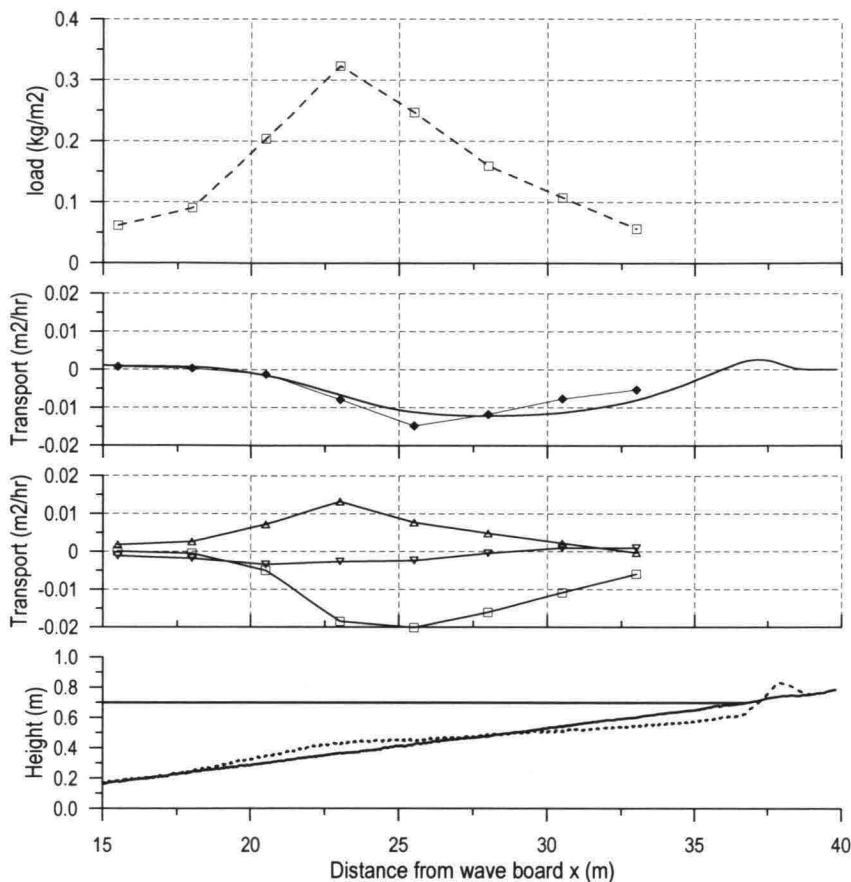


Figure 7 Time-mean load (upper plot), sediment transport (second plot) derived from profile deformation (line) and from flux profiles (diamond), transport from flux profiles (third plot) decomposed in short wave contribution (triangle up), long wave contribution (triangle down) and mean flow (square) and initial bed and bed after 30 hours (lower plot)

Transport obtained from flux profiles

In addition, the time-averaged transport rate has been computed as the time- and depth-averaged sediment flux, given by:

$$\langle q \rangle = \frac{1}{(t_2 - t_1)} \int_{t_1}^{t_2} \int_{z_s}^{z_r} u(x, z, t) c_v(x, z, t) dz dt, \quad (3)$$

where z_s is formally the water level and practically the elevation of the highest measuring point, u the horizontal velocity and c_v the volume concentration of sediment. Figure 7 shows, besides the net transport rate inferred from profile

deformation, the transport rates computed from integration of the fluxes. The agreement between the two is striking; apparently we are able to account for the majority of the transport when using the measured suspended sediment fluxes. Note that for the two most shoreward measuring locations the concentration does not completely vanish for the highest measuring point, such that we can expect that at those locations the transport rates inferred from the flux profiles underestimate the actual transport rates. This however cannot explain the shift in the maximum transport, which for the transport rates inferred from the flux profiles occurs at deeper water.

Transport at the various flow scales

Separation of velocity and concentration into time scales of waves, wave groups and undertow yields:

$$\langle q \rangle = \frac{1}{(t_2 - t_1)} \int_{t_1}^{t_2} \int_{z_b}^{z_s} \langle u \rangle \langle c_v \rangle + u_{lo} c_{v,lo} + u_{hi} c_{v,hi} dz dt, \quad (4)$$

when assuming that velocity and concentration on the different time scales are uncorrelated.

Throughout this paper, the first term which is related to the time-averaged current and concentration, is referred to as mean flow related transport. The second and the third term are called long wave related transport and short wave related transport, respectively. The respective contributions to the net transport rates are shown in the third plot of Figure 7. It can be seen that the mean flow related transport is the most significant component for the larger part of the profile, especially in the outer breaker zone where the wave-generated undertow is combined with a high suspended load. Seaward of the point of initial breaking however, the small but dominant short wave related transport results in a small onshore transport. It can be concluded that outside the breaker zone the prediction of the transport direction by any transport formulation is critically dependent on the proper representation of relatively small terms. It can be seen that the trend in the total transport only partly resembles the trend in the total fourth velocity moment. Due to mainly the strong vertical gradients in the mean flow however, the fourth velocity moment (Figure 5) is strongly height-dependent.

The second term is related to the correlation between sediment concentration and long wave motions. Since the slow variations in sediment concentration, stirred up by the high frequency waves, are coupled to the variations in wave energy on the wave group scale, the phase shift between the long wave and the short wave variance determines whether the resulting long wave related transport is onshore or offshore directed. At deeper water the cross-correlation between long wave and short wave variance is negative (see Figure 3), such that the highest high frequency waves and therefore the highest sediment concentrations occur during the offshore directed low frequency motion resulting in an offshore transport. An onshore long wave related transport is found for those locations for which the cross-correlation is positive. Note that in this reasoning, we have neglected the phase shift between short wave energy

and sediment concentration of the order of the peak frequency (see later on).

The third term is related to wave asymmetry and time lag effects between wave orbital velocity and concentration within the wave cycle. The increasing asymmetry about the horizontal plane in shoaling waves and the non-linear response of the concentration to the wave-induced bottom shear stress, results in a net onshore directed short wave related sediment transport, which may be reduced and even reversed due to phase lags between concentration and velocity.

Expansion of velocity moments

Despite the limitations of the energetics approach with respect to the assumption of an instantaneous response of the sediment concentration to a representative water velocity, a logical next step seems a comparison of the derived mean flow, long wave and short wave related sediment transport rates with the three components of the velocity moment in Equation (1). However, although sometimes regarded as such in literature, the relative contribution of the terms in Equation (1) to the total velocity moment does not formally reflect the relative amount of sediment transported by the mean flow, low frequency and high-frequency waves respectively, as defined in Equation (4). According to the energetics approach (Bailard, 1981), the suspended sediment transport is proportional to the fourth velocity moment $\langle u(t)|u(t)^3 \rangle$ reflecting that the water velocity $u(t)$ transports a suspended sediment load proportional to the energy dissipation in the flow described by $|u(t)^3|$. Analogously to Equation (4), we would then write $\langle u(t)|u(t)^3 \rangle$ as:

$$\langle u(t)|u(t)^3 \rangle = \langle u \rangle \langle |u^3| \rangle + \langle u_{lo} |u^3|_{lo} \rangle + \langle u_{hi} |u^3|_{hi} \rangle = \langle u \rangle \langle |u^3| \rangle + \langle u_{lo} |u^3| \rangle + \langle u_{hi} |u^3| \rangle \quad (5)$$

Assuming that $\langle u \rangle \ll u_{lo} \ll u_{hi}$ and u_{hi} is uncorrelated to $\langle u_{lo}^2 \rangle$ and $\langle |u_{lo}|^3 \rangle$, we approximate the mean flow, long wave and short wave related moment respectively by:

$$\langle u \rangle \langle |u^3| \rangle \approx \langle u \rangle \langle |u_{hi}^3| \rangle; \langle u_{lo} |u^3| \rangle \approx \langle u_{lo} |u_{hi}^3| \rangle; \langle u_{hi} |u^3| \rangle \approx \langle u_{hi} |u_{hi}^3| \rangle + 3 \langle u_{lo} |u_{hi}^3| \rangle + 3 \langle u \rangle \langle |u_{hi}^3| \rangle \quad (6)$$

Comparison of Equation (6) with Equation (1) shows that the relative contribution of the three terms in Equation (1) to the total velocity moment cannot be regarded as the part of the total transport by mean flow, long waves and short waves, respectively according to the separation in time-scales as applied in Equation (4) and (6).

VERTICAL PROFILES OF VELOCITY, CONCENTRATION AND FLUXES

Velocity and concentration profiles

Some characteristics of the vertical profile of velocity and concentration are shown in Figure 8 for a position shoreward of the breaker bar crest ($x = 255 \text{ m}$). The upper three plots show the profile of undertow, standard deviation of the low-pass filtered and

de-measured velocity and high-pass filtered velocity signal, respectively. In the lower three plots, the same parameters are shown for the concentration signal. The increase in standard deviation of the high-pass filtered velocity signal close to bed is likely to be related to the increased turbulence. The larger boundary layer of the longer waves is observed from the decrease of the standard deviation of the low-frequency signal towards the bed. Further it can be seen that both the high and low frequency part of the concentration signal are significant, the latter showing a stronger vertical gradient in the standard deviation.

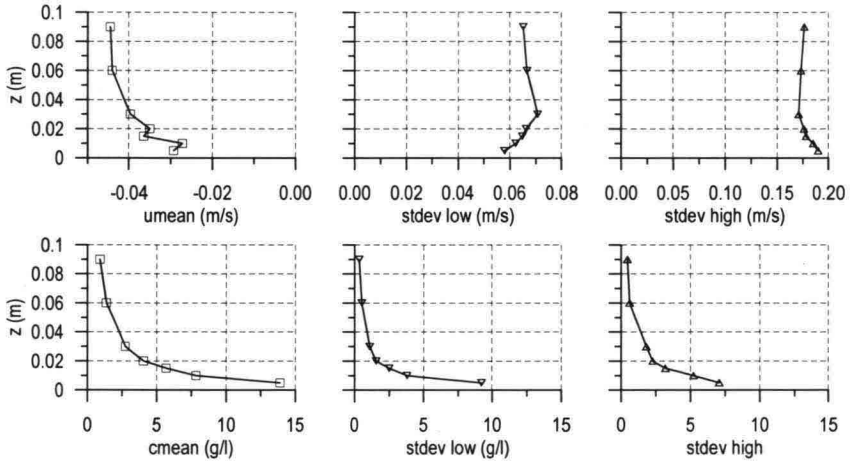


Figure 8 Velocity and concentration parameters at 25.5 m as a function of the distance from the ripple tops

Suspended sediment flux profiles

In Figure 9 time-averaged flux profiles are shown with a distinction between total fluxes and mean flow, long wave and short wave related fluxes defined in an identical matter as the separation of the transport rates in Equation (4). The upper plot and lower plot relate to $x = 20.5\ m$ and $x = 25.5\ m$, respectively. The latter is located around the point of maximum negative transport rates, whereas at the first location the total transport rate is very small but offshore directed.

At $x = 25.5\ m$ the onshore effect of the short wave related fluxes is greatly reduced by the long wave related flux, such that the total flux is similar to flux by the undertow. Higher up in the water column, the magnitude of the short wave component is larger than that of the long wave component such that a net onshore oscillatory flux occurs at higher levels. The relative contribution of the short waves is significantly larger at $x = 20.5\ m$ (in the shoaling region), which even results in an onshore directed total flux further from the bed. Very interesting is the decrease in the short wave component from about 2 cm above the ripple tops towards the bed, whereas the standard deviation of the high-pass filtered velocity signal increases towards the bed (not shown) analogous to the trend at $x = 25.5\ m$ shown in Figure 8. This is likely to be related to the fact that,

especially for the shorter waves, the time-averaged flux is critically dependent on time lag effects between wave orbital velocity and concentration within the wave cycle. Apparently, the phase lags are such that the net flux decreases towards the bed.

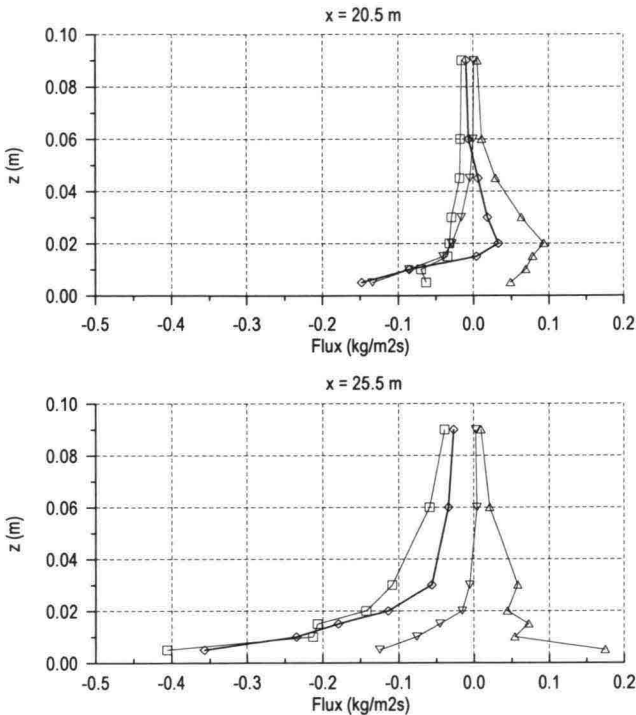


Figure 9 Total net suspended sediment fluxes (diamond) at $x = 20.5\text{ m}$ (upper plot) and $x = 25.5\text{ m}$ (lower plot) as a function of height above the ripple tops, decomposed in short wave (triangle up), long wave contribution (triangle down) and mean flow contribution (square)

Cross-spectral analysis

Cross-spectral analysis between velocity and concentration reveals the contribution to the net sediment flux and the phase relationships between velocity and concentration at any particular frequency (see Huntley and Hanes, 1987). The real part of the cross-spectrum, the co-spectrum, can be thought of as the product of velocity and concentration in a narrow frequency range divided by the frequency interval. The integral of the co-spectrum over all frequencies is then equal to the net sediment flux $\langle uc \rangle$. The magnitude of the cross-spectrum is the same, except that the signals are shifted such that the phase shift between the u and c at each frequency is zero. It therefore reflects a maximum sediment flux at each frequency in the imaginary situation that no phase lag exists at that particular frequency and is therefore called potential flux magnitude in this paper. Figure 10 shows the co-spectrum and

magnitude of the cross-spectrum for a single measurement at $x = 20.5 \text{ m}$ and $z_{rel} = 0.5 \text{ cm}$ corresponding to the upper plot of Figure 9.

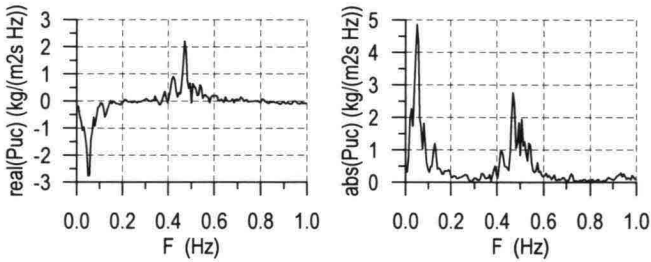


Figure 10 Co-spectrum and magnitude of the cross-spectrum for a single measurement at $x = 20.5 \text{ m}$ and $z_{rel} = 0.5 \text{ cm}$

It can be seen that in the high-frequency range ($> 0.25 \text{ Hz}$), the primary contribution to the net flux is concentrated around the peak frequency and that the magnitude of the actual short wave flux is significantly smaller than the magnitude of the potential flux. Figure 11 shows the time-averaged actual and potential short wave flux determined from integration over the high frequency range of the co-spectrum and the magnitude of the cross-spectrum respectively as a function of the height above the ripple tops. From this figure it is clear that the actual net short wave flux is critically dependent on the phase shifts between velocity and concentration at each frequency and that in this particular situation this results in a decreasing ratio of actual flux over potential flux when approaching the bed. The latter may be related to the suspension process over rippled beds where sediment is entrained by vortices and subsequently ejected in the flow (Osborne and Vincent, 1996).

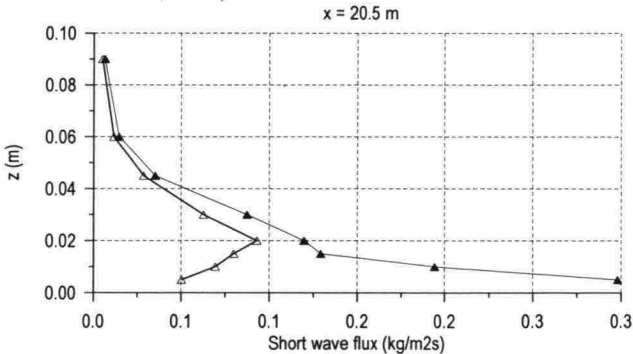


Figure 11 Short wave flux; actual flux (open triangles), potential flux (filled triangles)

As mentioned before, at $x = 20.5 \text{ m}$ a large negative cross-correlation between long wave velocity and slowly varying velocity variance can be observed. It was found that the phase shift between the long wave velocity and the highest wave in a group for the greater part determines the difference between the magnitude of the actual and potential flux in the low-frequency range. The phase shift between slowly varying

short wave velocity variance and sediment concentration was found to be of the order of the peak frequency, which means that the highest sediment concentrations lag one peak period behind the highest wave in the group. This is consistent with findings in earlier field and laboratory studies (for instance Jiménez, 1998).

CONCLUSIONS

The data gathered during flume experiments with random waves normally incident on a dissipative beach are presented. Detailed measurements of instantaneous fluid velocities and sediment concentrations were made resolving the spatial structure (in both horizontal and vertical direction) of the velocity and concentration fields. The set-up of the measurement programme was so as to enable the identification of the spatial correlation (in both horizontal and vertical direction) of concentration, the time-dependent near-bottom response of the concentration to water velocity and the contribution of the various velocity components to the sediment fluxes. In the ongoing analysis, it is found that the oscillatory contribution to the suspended sediment transport, dominated by the short wave transport, cannot be neglected. Further, the net oscillatory fluxes are found to be critically dependent on the phase shifts between velocity and concentration at each frequency.

ACKNOWLEDGEMENTS

This work is undertaken in the SAFE project, in the framework of the EU-sponsored Marine Science and Technology Programme (MAST-III), under contract no. MAS3-CT95-0004. It is cosponsored by the Dutch Ministry of Transport and Public Works (Rijkswaterstaat).

REFERENCES

- Bailard, J.A., 1981. An energetics total load sediment transport model for a plane sloping beach. *J. of Geophys. Res.*, Vol. 86: C11: 10,938-10,954.
- Bosman, J. J., van der Velden, E. T. J. M. & Hulsbergen, C. H., 1987 Sediment Concentration Measurement by Transverse Suction. *Coastal Engineering*, 11:353-370.
- Huntley, D.A. and D.M. Hanes, 1987. Direct measurement of suspended sediment transport. *Proceedings Coastal Dynamics 1987*, ASCE: 723-737.
- Jiménez, J.A., Sánchez-Arcilla, A. and Rodríguez, G., 1998. Sediment resuspension under non-breaking waves. Predicting sediment "pulses" as a function of groupiness. *Proc. 26th ICCE*, ASCE (in press).
- Roelvink, J.A. and Stive, M.J.F., 1989, Bar-generating offshore flow mechanisms on a beach. *Journal of Geophysical Research*, Vol. 94, No. C4: 4785-4800.
- Koomans, R. L., Bosboom, J., Meijer, R. J. de and Venema, L. B., 1999. Effects of density on cross-shore sediment transport. *Proceedings of Coastal Sediments 99*.
- Klopman, G., 1995. Active wave absorption, Digital control systems for wave channels based on linear wave-theory. Report on desk study, Part II. *Report H1222*, WL|DELFT HYDRAULICS
- Klopman, G., 1998. *Personal communication*
- Osborne, P.D. and Vincent, C.E., 1996. Vertical and horizontal structure in suspended sand concentrations and wave-induced fluxes over bedforms. *Marine Geology*, Vol. 132, pp: 195-208.